



# Source characteristics, site effects from spectral analysis of ground motions in 2016 Kaikoura seismic sequence

H.W. Wang, Y.F. Ren, Y. Zhou, R.Z. Wen & Q.L. Li

Institute of Engineering Mechanics, China Earthquake Administration; Key Laboratory of Earthquake Engineering and Engineering Vibration of China Earthquake Administration, Harbin, China.

### **ABSTRACT**

The spectral inversion technique was used to investigate the source characteristics and site effects of a total of 2445 S-wave Fourier amplitude spectra recorded at 126 GeoNet stations in 148 earthquakes from the  $M_{\rm w}7.8$  Kaikoura seismic sequence. The seismic moment, corner frequency, and stress drop for each earthquake were estimated based on the inverted source spectra. The seismic moment is inversely proportional to the cube of the corner frequency, implying this seismic sequence within the investigated magnitude range followed self-similarity. The stress drop varied predominantly from 0.2 to 6.0 MPa with a logarithmic mean of 1.25 MPa, and it did not show any evidence of dependence on magnitude size and focal depth. The features of the site responses of the 126 strong-motion stations inverted in this study were investigated to reveal the following results. Linear relationships between the site amplification and site characteristic parameters,  $V_{\rm S30}$  and  $T_{\rm site}$  at each frequency point of 0.5–3.0 Hz were regressed with correlation coefficients of 0.5–0.8, indicating that site amplification correlates moderately with both parameters. Site amplification in the Wellington region exhibited strong correlation with the geological and geotechnical characterization, e.g., the depth of the soil deposit. Strong site amplification appeared considerable in the Christchurch Central Business District.

## 1 INTRODUCTION

The 2016  $M_w$ 7.8 Kaikoura earthquake was the largest earthquake recorded in New Zealand since the 1855  $M_w$ 8.2 Wairarapa earthquake (epicenter shown in Fig. 1), and it has aroused great concern among earthquake scientists and engineers worldwide. The Kaikoura earthquake initiated in the Waiau Plains of North Canterbury, where the extremely complex tectonic regime is characterized by the transition from the

southern Hikurangi subduction zone to the oblique continental convergence dominated by the strike-slip Alpine fault. Investigating the source characteristics (e.g., scaling relations of source parameters) of this earthquake sequence constitutes one of the vital procedures necessary for re-evaluating seismic hazard near seismogenic faults.

The severe ground shaking in this Kaikoura earthquake generated notable surface responses such as extreme rupture displacement of up to 9–11 m horizontally and 6–8 m vertically (Litchfield *et al.* 2016), tens of thousands of landslides (Dellow *et al.* 2017), and widespread liquefaction (Cubrinovski *et al.* 2017). The city of Wellington suffered considerable societal impact, even though it was  $\sim$ 60 km from the causative earthquake rupture. One of the reasons could have been site amplification of long-period ground motions (T = 1-2 s), which at some locations exceeded the current 500-year return period design level of ground motion (Bradley *et al.* 2018). These observations emphasize the importance of appropriate consideration of site effects in design codes.

This study conducted comprehensive analyses of both the source characteristics of the Kaikoura earthquake sequence and the site effects revealed at many strong-motion stations using the spectral inversion method, based on the rich strong-motion recordings provided by GeoNet. The similar studies were performed by Oth and Kaiser (2014), Kaiser *et al.* (2013) to simultaneously analyze the source characteristics, path attenuation and site effects in the 2010–2011 Canterbury earthquake sequence. The source parameters were estimated from the inverted source spectra to study the source-scaling relations of this earthquake sequence. The site effects considered in this study were site amplification and predominant frequency within this region, especially near Wellington and Christchurch.

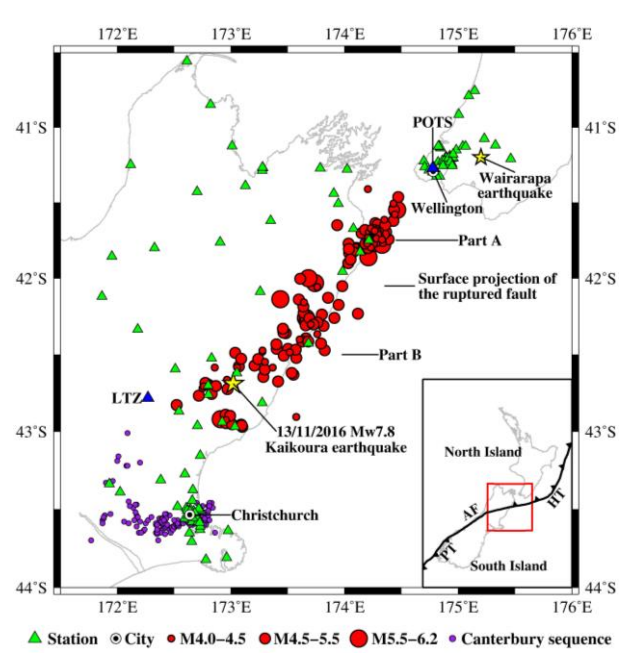


Figure 1: Locations of earthquakes and strong-motion stations considered in this study. Two stars indicate the epicenters of the 2016  $M_w$ 7.8 Kaikoura earthquake and the 1855 Wairarapa earthquake, respectively. The blue triangles represent two reference stations in the inversion. The purple circles indicate the epicenters of the 2010–2011 Canterbury earthquake sequence used by 0th and Kaiser (2014).

# 2 DATASET

GeoNet released 12,313 strong-motion recordings collected at 264 stations in 367 earthquakes with local magnitudes ( $M_L$ ) of 4.00–6.26, which occurred as part of the Kaikoura earthquake sequence from November 13, 2016 to March 1, 2017. This study used a dataset constructed according to the following criteria: (1)  $d \le$ 

Paper 232 – Source characteristics, site effects from spectral analysis of ground motions in 2016 Kaikoura...

30 km; (2)  $20 \text{ km} \le R \le 200 \text{ km}$ ; (3)  $2 \text{ cm/s}^2 \le \text{PGA} \le 100 \text{ cm/s}^2$ ; and (4) each selected earthquake should be recorded by at least four stations, each of which should collect at least four recordings that match criteria (1), (2), and (3). Overall, 2445 strong-motion recordings from 148 earthquakes for  $M_L4.02-6.16$  recorded at 126 strong-motion stations were assembled for the inversion. The geographical locations of the stations and earthquakes considered are marked in Figure 1.

Recordings were processed using a Butterworth band-pass filter: 0.25-25.0 Hz for recordings in earthquakes with  $M_L < 4.5$ , 0.2-25.0 Hz for  $4.5 \le M_L < 5.5$ , and 0.1-25.0 Hz for  $M_L \ge 5.5$ . The S-wave window was extracted according to the Husid function (Husid 1967) and the cumulative root-mean-square function (McCann & Shah 1979). The Fourier amplitude spectra for the tapered and zero-padded S waves were calculated and smoothed. The root-mean-square of the Fourier amplitude spectra from two horizontal S waves was adopted to represent the horizontal ground motion.

### 3 METHODOLOGY

The generalized inversion technique (GIT) was adopted to separate simultaneously the S-wave Fourier amplitude spectra into source spectra, path attenuation, and site responses. The convolution of the three contributions in the time domain can be expressed as a simple multiplication in the frequency domain:

$$O_{ij}(f, M_i, R_{ij}) = S_i(f, M_i) \cdot P_{ij}(f, R_{ij}) \cdot G_j(f),$$
(1)

where  $O_{ij}(f, M_i, R_{ij})$  represents the acceleration Fourier amplitude spectrum at frequency f obtained at the j-th station resulting from the i-th earthquake with magnitude  $M_i$ ,  $R_{ij}$  is the hypocentral distance,  $S_i(f, M_i)$  is the source acceleration spectrum of the i-th event, and  $G_j(f)$  accounts for the site response of the j-th station. Here,  $P_{ij}(f, R_{ij})$  is the attenuation operator involving geometrical spreading, anelastic and scattering attenuation, and refracted arrivals, which can be simply expressed as

$$P_{ij}(f) = GS(R_{ij}) \cdot \exp\left(\frac{-\pi f R_{ij}}{\beta_s Q_s}\right),\tag{2}$$

where  $Q_S$  stands for the frequency-dependent S-wave quality factor,  $\beta_S$  is the shear-wave velocity set to 3.7 km/s.  $GS(R_{ij})$  represents the geometrical spreading. A hinged trilinear GS model given by Atkinson and Mereu (1992) was used in this study.

The singular value decomposition method was adopted to solve Eq. (1). In order to eliminate the trade-off between the source and the site terms, two stations were selected as reference sites, POTS and LTZ (highlighted in Fig. 1). Both stations were installed on rock (site class B in the NZS1170.5) with  $V_{S30} = 1000$  m/s derived from the GeoNet database of site metadata (Kaiser *et al.* 2017). The H/V spectral ratios of observed recordings in the Kaikoura earthquake sequence at both stations indicate the small (< 2.0) and flat site amplifications. Furthermore, some studies (e.g., Bradley *et al.* 2018) also considered the POTS station as the reference site for the site effect analyses using the standard spectral ratio method. The site responses at both reference sites were characterized by 2.0 (considering the amplification of the free surface).

# 4 SOURCE CHARACTERISTICS

The source displacement spectra of the 148 earthquakes considered in this study are shown in Figure 2(a). The spectral shapes at low-to-intermediate frequencies are mostly in good agreement with the omega-square source model (Brune 1970). However, rapid decay can be observed at high frequencies. In this study, we just adopted the simple multiplicative  $f_{\text{max}}$  filter (Boore 2003) to account for the high-frequency decay. The source displacement spectrum can be given by

$$S(f) = \frac{R_{\Theta\Phi}VF}{4\pi\rho_S \beta_S^2 R_0} \cdot \frac{M_0}{1 + (f/f_c)^2} \cdot [1 + (f/f_{\text{max}})^8]^{-1/2},\tag{3}$$

Paper 232 – Source characteristics, site effects from spectral analysis of ground motions in 2016 Kaikoura...

where  $M_0$  and  $f_c$  are the seismic moment and corner frequency, respectively. Here,  $R_{\Theta\Phi}$  accounts for the average radiation pattern over a suitable range of azimuths and take-off angles and it was set equal to 0.55 (Boore & Boatwright 1984),  $V = 1/\sqrt{2}$  represents the proportion of S-wave energy contained in the horizontal component, F is the amplification of the free surface, fixed to 1.0 because of its consideration in the site response,  $R_0 = 1$  km is the reference distance, and  $\rho_s = 2.7$  g/m<sup>3</sup> is the density near the source.

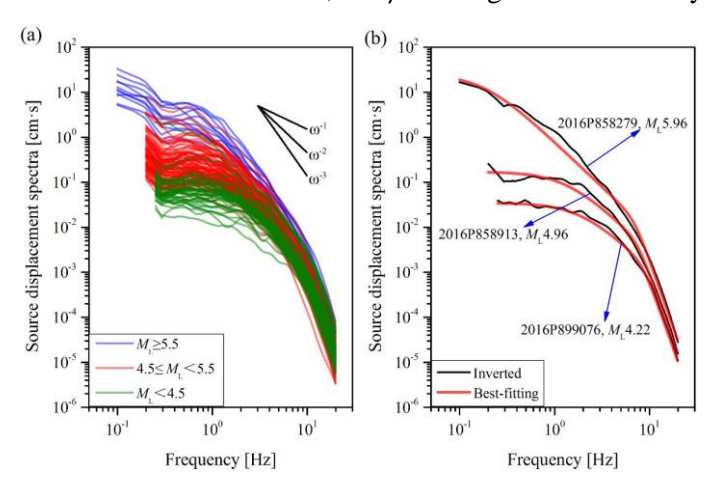


Figure 2: (a) Inverted source spectra for all 148 earthquakes considered in this study. The source spectra were separated into three groups considering three ML ranges. (b) Best-fitting theoretical source spectra for three typical events at different magnitude bins.

A grid-searching technique was adopted to obtain the best-fitting  $M_0$ ,  $f_c$ , and  $f_{max}$  for each event (*i*) under the condition that the theoretical source spectrum expressed by Eq. (3) showed the smallest deviations to the inverted source spectrum across the entire frequency range of 0.5–20.0 Hz. Figure 2(b) shows the best-fitting theoretical source spectra for several typical events at different magnitude bins. Perfect matches are observed between the inverted and theoretical spectra. Based on the optimum  $M_0$  and  $f_c$ , the stress drop can be estimated using the following relation (Brune 1970):

$$\Delta\sigma = \frac{7M_0}{16} \cdot \left(\frac{2\pi f_c}{2.34\beta_c}\right)^3,\tag{4}$$

The scaling characteristics for the Kaikoura earthquake sequence in the form of the  $M_w$ – $f_c$  plot are shown in Figure 3(a). The values of  $M_0$  and  $f_c$  vary from  $6.68\times10^{14}$  to  $7.67\times10^{17}$  Nm and from 0.19 to 2.61 Hz, respectively. If earthquakes follow self-similarity, the value of  $M_0$  is approximately inversely proportional to the cube of  $f_c$ , i.e.,  $M_0 \propto f_c^{-3}$ , which also means the stress drop is constant and independent of magnitude size. Studies by Allmann and Shearer (2009), Oth *et al.* (2010) among others, all confirmed the self-similarity of global earthquakes. However, some other studies have obtained conflicting results, in which self-similarity is broken down in some specific earthquake sequences (e.g., Tusa *et al.* 2006; Oth *et al.* 2013; Pacor *et al.* 2016). Kanamori & Rivera (2004) proposed the parameter  $\varepsilon$  in the formula  $M_0 \propto f_c^{-(3+\varepsilon)}$  to reflect quantitatively the deviations from self-similarity. In the case of  $\varepsilon = 0$ , self-similarity is followed perfectly, while the case of  $\varepsilon > 0$  ( $\varepsilon < 0$ ) indicates an increasing stress drop with increasing (decreasing) magnitude. In this study, a value of  $\varepsilon = 0.02 \pm 0.08$  was determined from the regression analysis, implying sound self-similarity for the Kaikoura earthquake sequence within the magnitude range of  $M_L$  4.02–6.16. Interestingly, in the 2010–2011 Canterbury earthquake sequence (shown in Fig. 1), it was also confirmed that the stress drop scaling with earthquake size was nearly self-similar (Oth & Kaiser, 2014).

The  $\Delta\sigma$  values for the Kaikoura earthquake sequence follow a lognormal distribution, as shown in Figure 3(b), and they vary predominantly from 0.2 to 6.0 MPa with a logarithmic mean of 1.25 MPa. These values are overall lower than the 2010–2011 Canterbury earthquake sequence with a logarithmic mean of ~5 MPa (Fig. 3(a)). The mean stress drop of the Kaikoura earthquake sequence is also lower than the median of

Paper 232 – Source characteristics, site effects from spectral analysis of ground motions in 2016 Kaikoura...

global interplate earthquakes, 3.31 MPa (Allamnn & Shearer 2009). No evidence was observed regarding the dependence of the stress drop on either magnitude or focal depth, as shown in Figures 3(c)–(d).

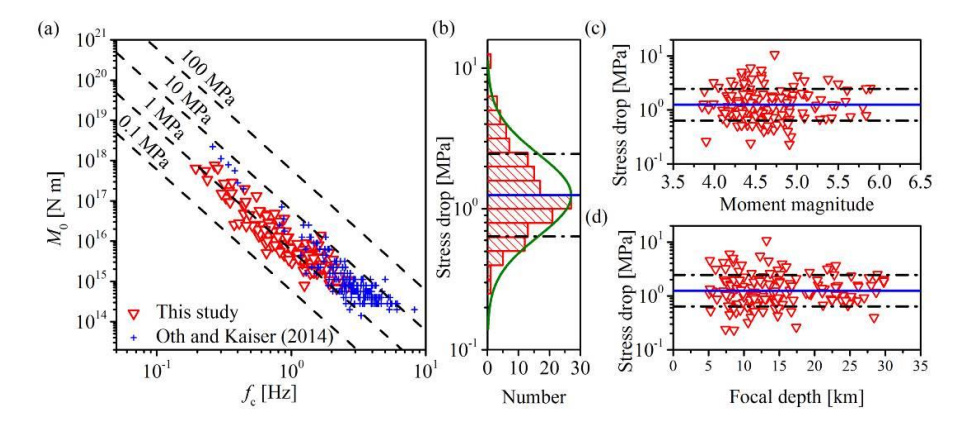


Figure 3: (a) Plots of the seismic moment  $M_0$  vs. corner frequency  $f_c$ . The  $M_0$ – $f_c$  plots for the 2010–2011 Canterbury earthquake sequence provided by Oth and Kaiser (2014) were compared with our results. (b) Histogram of the stress drop values on the base-10 logrithmic scale, and the best-fitting lognormal distribution function. (c) Stress drop vs. moment magnitude. (d) Stress drop vs. focal depth.

### 5 SITE EFFECTS

The site response functions at 0.5–20.0 Hz for the 126 strong-motion stations were obtained. The bootstrap analysis (Oth *et al.* 2008) was performed to calculate the standard deviation of site response.

To detect the correlations between the site amplification and the site parameters, e.g.,  $V_{\rm S30}$  and  $T_{\rm site}$ , 24 stations with credible values of  $V_{\rm S30}$  (quality levels of  $Q_{\rm 1}$  and  $Q_{\rm 2}$ ) and 50 stations with credible values of  $T_{\rm site}$  (quality levels of  $Q_{\rm 1}$  and  $Q_{\rm 2}$ ) were included, respectively. Taking 0.5 Hz as an example in Figures 4(a)–(b), good correlations between the site amplification (Amp.) and either  $V_{\rm S30}$  or  $T_{\rm site}$  can be observed clearly with both able to be expressed as a linear relationship:

$$\ln(Amp.) = a + b \cdot \ln(V_{S30})$$
(5)

and

$$ln(Amp.)=a+b\cdot ln(T_{site}), (6)$$

The linear correlation coefficients at each frequency from 0.5 to 20.0 Hz for the  $Amp.-V_{S30}$  and  $Amp.-T_{site}$  regressions were computed and shown in Figure 4(c). The  $Amp.-V_{S30}$  relationship shows negative correlation at low-frequency band but positive correlation at high-frequency band. However, the  $Amp.-T_{site}$  relationship follows the opposite trend. Moderate correlations (correlation coefficients from 0.5 to 0.8 and -0.8 to -0.5) can be observed at the low-frequency band ( $<\sim$ 3.0 Hz) for both relationships. Weak correlations are also evident at the high-frequency band ( $<\sim$ 3.0 Hz), but the relationship is almost independent at the intermediate-frequency band ( $<\sim$ 3.0-8.0 Hz). Actually, negative correlation between the site amplification and  $V_{S30}$  at the low-frequency band has been reported in many studies, e.g., at a band of 0.5-2.5 Hz by Dutta et al. (2003), 0.4-1.0 Hz by Hassani et al. (2011), and 0.5-1.0 Hz by Tsuda et al. (2010). In addition, the independence at the intermediate-frequency band has also been reported previously, e.g., at a band of 3.0-7.0 Hz by Dutta et al. (2003) and 2.5-6.0 Hz by Hassani et al. (2011). According to the least squares regression analysis, the values for the slope (et) and the intercept (et) for the relationships of et0.5 and et1 in the relationship of et2.5 vary from 5.75 to 10.89 and from -1.65 to -0.74 at the low-frequency band (0.5-3.0 Hz), respectively, which are approximately in good agreement with those provided by Dutta et2. (2003).

Paper 232 – Source characteristics, site effects from spectral analysis of ground motions in 2016 Kaikoura...

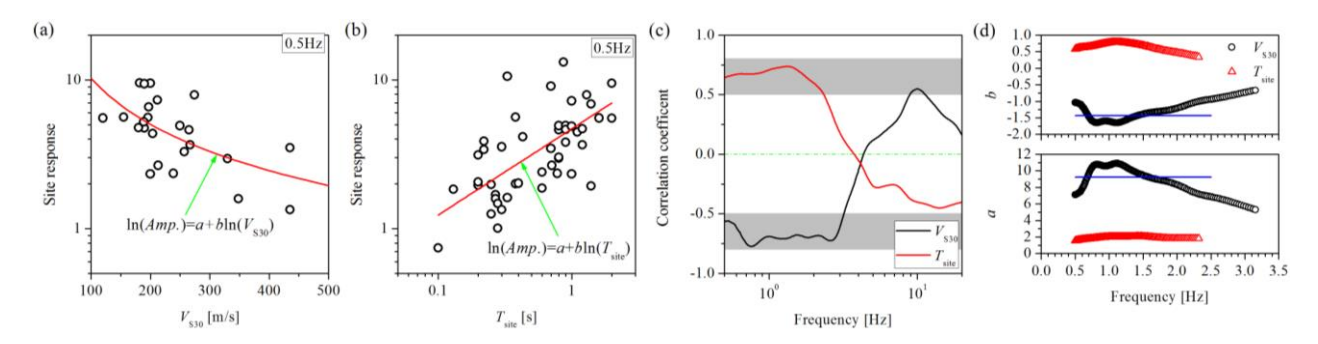


Figure 4: Site amplification (Amp.) at 0.5 Hz vs. (a)  $V_{S30}$  and (b) fundamental site period  $T_{site}$ . The solid lines indicate the best-fitting relationships between the two parameters. (c) Linear correlation coefficients for the linear regressions of Amp.– $V_{S30}$  and A

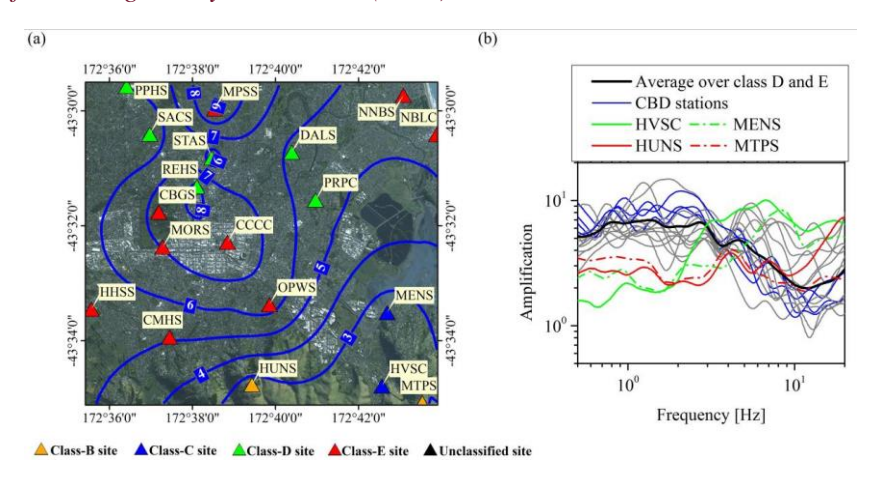


Figure 5: (a) The contours (blue lines) for average site amplification at low-frequency band (0.5–3.0 Hz) in the Christchurch city. (b) The site response functions at stations shown in panel (a).

The contour map of the average site amplification over 0.5–3.0 Hz in Christchurch was shown in Figure 5(a). The site amplifications in south Christchurch ( $\sim 3-5$ ) were smaller than the north ( $\sim 6-8$ ), which might be inferred as the result of shallow basement rock depth in south associated with uplift during Miocene volcanism. Most stations situated on the Christchurch sedimentary basin are classified as class D and E sites (see Fig. 5(a)) covered by the soft soils ( $V_{S30}$  < 250 m/s). Only four stations are classified as class B and C sites. They are stations HVSC and MENS (class C) near the north edge of the Port Hills and stations HUNS and MTPS (class B). The site amplifications of these stations shown in Figure 5(a) were plotted in Figure 5(b). For both class B sites, the flat amplification function shows weak site responses (~3.0). The larger amplifications at frequencies from 2 to 8 Hz, exhibited at station HVSC than at station MENS, could be interpreted by the basin-edge effect, which was also observed in the 13 June 2011 M<sub>w</sub>6.0 Christchurch earthquake (Bradley, 2016). The amplifications at frequencies lower than ~ 3.0 Hz for those stations (class D and class E sites) within the sedimentary basin are consistently larger than the southeastern stations (class B and class C sites), which illustrates the effects of the thick sequence of soil layer, previously observed in the Canterbury seismic sequence (Bradley & Cubrinovski 2011). It should be noted that stronger amplifications appeared in the Christchurch Central Business District (CBD), i.e., close to stations CBGS, CCCC, REHS, and MORS (see Fig. 5(a)). The amplifications at low frequencies for these four stations are larger than the average values over all class D and class E sites, as shown in Figure 5(b).

In central Wellington, the site effects of 14 strong-motion stations were analyzed in detail for the potential needs of seismic design. As for Christchurch city, the contour for the average site amplification over

Paper 232 – Source characteristics, site effects from spectral analysis of ground motions in 2016 Kaikoura...

frequencies of 0.5–3.0 Hz was calculated using the tension spline interpolation method (Fig. 6(a)). Amplification gradually increased from the western highlands to the eastern coasts in the north. The spatial variation of site amplification shows approximate consistency with the contours of soil depth to bedrock and site period (see Maps 4 and 6 in Appendix 3 of Semmens *et al.* (2010)), indicating larger site amplification in regions with deeper soil layers.

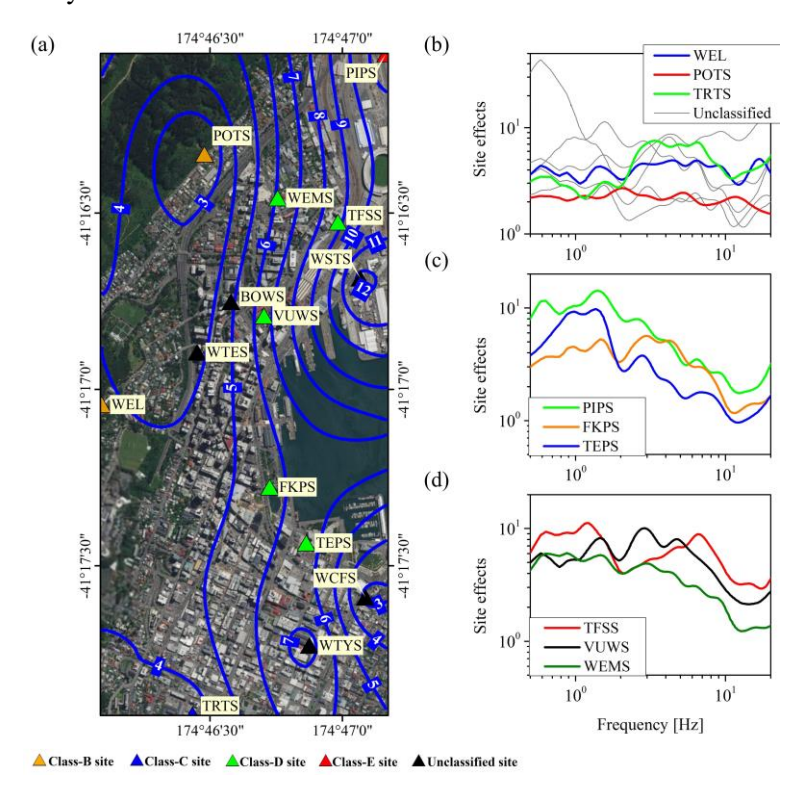


Figure 6: (a) The contours (blue lines) for average site amplification at low-frequency band (0.5–3.0 Hz) in Wellington city. (b) The site amplification functions at rock (WEL and POTS), class C (TRTS) and unclassified-site stations. (c) The site amplification functions at three reclaimed sites. (d) The site amplification functions at three alluvial-deposit sites.

According to the GeoNet database of site metadata (Kaiser et al. 2017), two rock stations, POTS and WEL, were classified as class B sites. Station PIPS on the reclamation overlying the alluvial deposits was classified as class E site. Two stations on the reclamation (TEPS, FKPS) and three stations on alluvial deposits (TFSS, VUMS, and WEMS) were classified as class D sites. Station TRTS on the south was classified as class C site. The site classes for the remaining five stations were unclassified. The site amplifications of these stations shown in Figure 6(a) were plotted in Figures 6(b)–(d). Fig. 6(b) illustrates the weak and flat site amplifications for both rock sites, ~2.0 at station POTS and ~3.5 at station WEL. The class C site (TRTS) exhibits larger amplifications than both rock sites at 3–7 Hz. The amplifications at the three reclaimed sites (PIPS, TEPS, and FKPS) indicate notable differences (Fig. 6(c)). The largest amplifications occur at station PIPS at 0.5–20.0 Hz. Compared with the station FKPS, the station TEPS shows higher amplifications at low frequencies below ~2.0 Hz, but lower amplifications at high frequencies over ~2.0 Hz. As described by Bradley et al. (2017) and Bradley et al. (2018), the station PIPS generally recorded the strongest spectral amplitudes in central Wellington in the Kaikoura earthquake, the station FKPS recorded the higher shortperiod ( $< \sim 0.7$  s) but smaller long-period ( $> \sim 0.7$  s) spectral amplitudes than the observations at station TEPS. The variations of site amplification among the three stations mirror the observed spectral amplitudes in the Kaikoura earthquake, and might be related to the sediment thicknesses, which were inferred to be approximately 60 m at FKPS, 120 m at TEPS and ~200 m at PIPS (Semmens et al. 2010). For the three stations on alluvial deposits, station WEMS exhibits smaller site amplifications than the other two stations

Paper 232 – Source characteristics, site effects from spectral analysis of ground motions in 2016 Kaikoura...

(TFSS and VUWS), (Fig. 6(d)). Coincidently, the lowest spectral amplitudes at periods less than 2.0 s were observed at this station (Bradley *et al.* 2017; Bradley *et al.* 2018).

# 6 CONCLUSION

The GIT was adopted to simultaneously separate the source, site, and path terms from the S-wave amplitude spectra of 2445 strong-motion recordings, which were obtained at 126 GeoNet strong-motion stations in the 148 aftershocks of the 2016 Kaikoura earthquake.

The values of  $M_0$ ,  $M_{\rm w}$ ,  $f_{\rm c}$ , and  $\Delta\sigma$  were derived for each event considered. The  $M_0$  and  $f_{\rm c}$  values varied from  $6.68\times10^{14}$  to  $7.67\times10^{17}$  Nm and from 0.19 to 2.61 Hz, respectively, and  $M_0$  was inversely proportional to the cube of  $f_{\rm c}$ , implying the earthquake self-similarity was followed by the Kaikoura sequence. The  $\Delta\sigma$  values predominantly varied from 0.2 to 6.0 MPa with a logarithmic mean of 1.25 MPa, significantly lower than those for the 2010–2011 Canterbury sequence (~5 MPa, Oth & Kaiser (2014)), and lower than the median for global interplate earthquakes (3.31 MPa, Allmann & Shearer (2009)). No evidence was observed regarding the dependence of  $\Delta\sigma$  on either magnitude or focal depth.

The site responses for 126 stations considered were estimated. Linear relationships between the site amplification and  $V_{\rm S30}$ ,  $T_{\rm site}$  at each frequency of 0.5–20.0 Hz were regressed. Results showed the correlation of site amplification with both parameters was moderate at low frequencies ( $< \sim 3.0$  Hz), weak at high frequencies ( $> \sim 8.0$  Hz), but almost independent at intermediate frequencies ( $\sim 3.0$ –8.0 Hz). Site amplifications in the Wellington region exhibited strong correlation with the geological and geotechnical characterization. Larger amplifications appeared in regions with deeper soil. Contour maps of site amplification in the Wellington and Christchurch regions exhibited considerable spatial variations. Largely frequency-dependent variations of site amplifications among stations with different site classes, which could explain their observed spectral amplitudes in the main shock (Bradley *et al.* 2018). Strong site amplification in the Christchurch CBD, consistent with previous studies, could explain the severe damage caused in this area in the past Christchurch earthquake.

# 7 REFERENCES

- Allmann, B.P. & Shearer, P.M. 2009. Global variations of stress drop for moderate to large earthquakes, *J. Geophys. Res.* 114, B01310.
- Atkinson, G.M. & Mereu, R.F. 1992. The shape of ground motion attenuation curves in southeastern Canada, *Bull. Seismol. Soc. Am.* 82, 2014–2031.
- Boore, D.M. 2003. Simulation of ground motion using the stochastic method, Pure appl. Geophys. 160, 635-676.
- Boore, D.M. & Boatwright, J. 1984. Average body-wave radiation coefficients, Bull. Seismol. Soc. Am. 74, 1615–1621.
- Bradley, B.A. 2016. Strong ground motion characteristics observed in the 13 June 2011  $M_{\rm w}6.0$  Christchurch, New Zealand earthquake, *Soil. Dyn. Earthq. Eng.* 91, 23–38.
- Bradley, B.A. & Cubrinovski, M. 2011. Near-source strong ground motions observed in the 22 February 2011 Christchurch earthquake, *Seismol, Res. Lett.* 82, 853–865.
- Bradley, B.A. Wotherspoon, L.M. & Kaiser, A.E. 2017. Ground motion and site effect observations in the Wellington region from the 2016  $M_{\rm w}$  7.8 Kaikoura, New Zealand earthquake, *Bulletin of the New Zealand Society for Earthquake Engineering* 50, 94–105.
- Bradley, B.A., Wotherspoon, L.M. Kaiser, A.E. Cox, B.R. & Jeong, S. 2018. Influence of site effects on observed ground motions in the Wellington region from the M<sub>w</sub>7.8 Kaikōura, New Zealand earthquake. *Bull. Seismol. Soc. Am.* 108, 1722–1735.
- Brune, J.N. 1970. Tectonic stress and the spectra of seismic shear waves from earthquakes, *J. Geophys. Res.* 75, 4997–5009.
- Cubrinovski, M. Bray, J.D. Torre, C. Olsen, M.J. Bradley, B.A. Chiaro, G. Stocks, E. & Wotherspoon, L. 2017. Liquefaction effects and associated damages observed at the Wellington Centreport from the 2016 Kaikoura
- Paper 232 Source characteristics, site effects from spectral analysis of ground motions in 2016 Kaikoura...

- Earthquake. Bulletin of the New Zealand Society for Earthquake Engineering 50, 152–173.
- Dellow, D. Massey, C. Cox, S. Archibald, G. Begg, J. Bruce, Z. Carey, J. Davidson, J. et al. (2017). Landslides caused by the M<sub>w</sub> 7.8 Kaikoura Earthquake and the immediate response. *Bulletin of the New Zealand Society for Earthquake Engineering* 50, 106–116.
- Dutta, U. Biswas, N. Martirosyan, A. Papageorgious, A. & Kinoshita, S. 2003. Estimation of earthquake source parameters and site response in Anchorage, Alaska from strong-motion network data using generalized inversion method, Phys. *Earth Planetary Int.* 137, 13–29.
- Hassani, B. Zafarani, H. Farjoodi, J. & Ansari, A. 2011. Estimation of site amplification, attenuation and source spectra of S-waves in the East-Central Iran, *Soil Dyn. Earthq. Eng.* 31, 1397–1413.
- Husid, P. (1967). Gravity effects on the earthquake response of yielding structures. Report of Earthquake Engineering Research Laboratory, Pasadena, California: California Institute of Technology.
- Kaiser, A.E. Houtte, C.V. Perrin, N.D. Wotherspoon, L. & Verry, G.H.M. 2017. Site characterisation of GeoNet stations for the New Zealand Strong Motion Database. *Bulletin of the New Zealand Society for Earthquake Engineering* 50, 39–49.
- Kaiser, A.E. Oth, A. & Benites, R.A. 2013. Separating source, path and site influences on ground motion during the Canterbury earthquake sequence, using spectral inversions, New Zealand Society for Earthquake Engineering Technical Conference, April 26–28, Wellington.
- Kanamori, H. & Rivera, L. 2004. Static and dynamic scaling relations for earthquakes and their implications for rupture speed and stress drop. *Bull. Seismol. Soc. Am.* 94, 314–319.
- Litchfield, N.J. Benson, A. Bischoff, A. Hatem, A. Barrier, A. Nicol, A. Wandres, A. Lukovic, B. Hall, B. & Gasston, C. 2016. 14th November 2016  $M_w$  7.8 Kaikoura earthquake. Preliminary surface fault displacement measurements, Version 2, GNS Science.
- McCann, M.W.J. & Shah, H.C. 1979. Determining strong motion duration of earthquakes, *Bull. Seismol. Soc. Am.* 69, 1253–1265.
- Oth, A. 2013. On the characteristics of earthquake stress release variations in Japan, *Earth and Planetary Science Letters* 377-378, 132–141.
- Oth, A. Bindi, D. Parolao, S. & Giacomo, D.D. 2010. Earthquake scaling characteristics and the scale-(in)dependence of seismic energy-to-moment ratio: Insights from KiK-net data in Japan. *Geophys. Res. Lett.* 37, L19304.
- Oth, A. Bindi, D. Parolai, S. & Wenzel, F. 2008. S-wave attenuation characteristics beneath the Veranca region in Romania: new insights from the inversion of ground-motion spectra, *Bull. Seism. Soc. Am.* 98, 2482–2497.
- Oth, A. & Kaiser A.E. 2014.Stress Release and Source Scaling of the 2010-2011 Canterbury, New Zealand Earthquake Sequence from Spectral Inversion of Ground Motion Data, *Pure appl. Geophys.* 171, 2767–2782.
- Pacor, F., Spallarossa, D. Oth, A. Luzi, L. Puglia, R. Cantore, L. Mercuri, A. D'Amoco, M. & Bindi, D. 2016. Spectral models for ground motion prediction in the L'Aquila region (central Italy): evidence for stress drop dependence on magnitude and depth, *Geophys. J. Int.* 204, 697–718.
- Semmens, S. Perrin, N.D. Dellow, G.D. 2010. It's our Fault Geological and Geotechnical characterisation of the Wellington Central Business District.GNS Science Consultancy Report 2010/176 June.2010.
- Tsuda, K. Koketsu, K. Hisada, Y. & Hayakawa, T. 2010. Inversion analysis of site responses in the Kanto Basin using data from a dense strong motion seismograph array, *Bull. seismol. Soc. Am.* 100, 1276–1287.